# Domain boundaries in incommensurate epitaxial layers on weakly interacting substrates

Yu Xiang, Songchun Xie, Zonghuan Lu, Xixing Wen, Jian Shi, Morris Washington, Gwo-Ching Wang, and Toh-Ming Lu

## COLLECTIONS

Paper published as part of the special topic on Novel Epitaxy of Functional Materials

View Online    Export Citation    CrossMark

## ARTICLES YOU MAY BE INTERESTED IN

# Domain boundaries in incommensurate epitaxial layers on weakly interacting substrates

Yu Xiang,[1,2] (ID) Songchun Xie,[1] (ID) Zonghuan Lu,[2] (ID) Xixing Wen,[1,2] (ID) Jian Shi,[2,3] (ID) Morris Washington,[1,2] (ID) Gwo-Ching Wang,[1,2] (ID) and Toh-Ming Lu[1,2,a)] (ID)

AFFILIATIONS

[1]Physics, Applied Physics and Astronomy Department, Rensselaer Polytechnic Institute, Troy, New York 12180, USA
[2]The Center for Materials, Devices, and Integrated Systems, Rensselaer Polytechnic Institute, Troy, New York 12180, USA
[3]Materials Science and Engineering Department, Rensselaer Polytechnic Institute, Troy, New York 12180, USA

**Note:** This paper is part of the Special Topic on Novel Epitaxy of Functional Materials.
[a)]**Author to whom correspondence should be addressed:** lut@rpi.edu

## ABSTRACT

There has been increasing interest in the fabrication of thin film materials with mixed dimensions, in particular, 2D to 3D and 3D to 2D heterostructures. Often, if the interface interaction is weak, the lattice matching criterion between the substrate and overlayer can be lifted. If the overlayer lattice is completely relaxed, it can form an incommensurate film on the mismatched substrate. In this work, we show that domain boundaries are inherent in the incommensurate epitaxial films due to random nucleation sites of domains in an overlayer. The nature and origin of the incommensurate domain boundaries are different from the conventional dislocation boundaries that come from the relaxation of strain due to film–substrate lattice mismatch. We propose that the formation of such domain boundaries can be studied through Voronoi tessellation. Using a case study of monolayer $WS_2$ on sapphire (2D on 3D), we show the formation of domain boundaries that compared well with a recent experiment reported in the literature. In the Voronoi tessellation, we also show quantitatively that the average domain size depends on the density of nucleation sites. The conclusion of this case study may be generalized to any incommensurate epitaxial films when the interface interaction is weak.
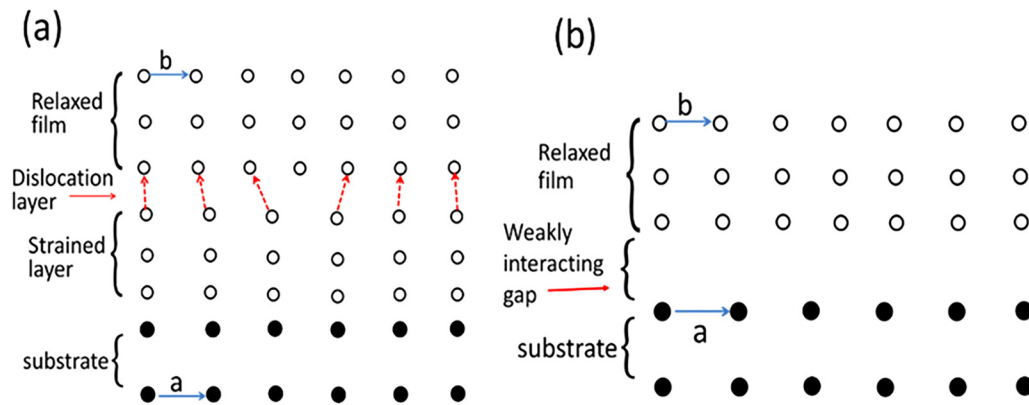
## I. INTRODUCTION

Thin film devices, the foundation of integrated circuit (IC) applications, are deeply embedded into modern life. To date, most high-performance electronic and optoelectronic devices are made of single-crystal films grown on single-crystal substrates.[1] A high-quality film hetero-epitaxially grown on a single-crystal substrate requires a good lattice matching between the film and the substrate. Because of this restriction, only limited combinations of materials can be utilized in a heteroepitaxy. Conventionally, for a covalent material system with a large lattice mismatch, the strong chemical interaction through charge sharing (such as covalent bonds) at the interface would produce a strained interfacial layer. The strain would propagate into the growing film and generate various defects such as dislocations, voids, and faults when the film reaches a critical thickness so that the growth front of the film would be relaxed to give a lattice constant closer to the intrinsic value of the film. Figure 1(a) illustrates schematically the phenomenon during the growth of a heteroepitaxial film with a large lattice mismatch ($b < a$) at the instance where the dislocation layer is generated. Typically, the dislocation core would propagate downward to the interface to further relax the film.[1]

To overcome this limitation of lattice mismatch, recently, there has been considerable interest in growing epitaxial films on single-crystal substrates through weak interactions such as van der Waals (vdW) forces.[2,3] The concept of van der Waals epitaxy (vdWE) has been around for over half a century.[4] Earlier works were focused on the growth of inert gases such as Ar or Xe on graphite.[5–7] For an inert gas, the condensation and epitaxy on a substrate typically occur at very low temperatures. Later, the idea of vdWE was extended to the epitaxial growth of other materials such as layered materials.[2,8] In contrast to the conventional chemical epitaxy where sharing or transferring of electrons occurs at the film–substrate interface, vdWE is believed to be based on the Coulombic force through long-range dipole interactions. Since

**FIG. 1.** (a) A schematic showing the formation of a dislocation layer during chemical heteroepitaxy of a film with a large lattice mismatch with respect to the single-crystal substrate. The unit lengths $b$ and $a$ are for overlayer and substrate, respectively. (b) A relaxed, incommensurate film epitaxially grown on a substrate through a van der Waals gap.

there is no "dangling bond" at the interface under weak vdW forces, the requirement of lattice matching to grow a high-quality film in conventional chemical epitaxy may be lifted and an epitaxial film can be grown even when the lattice mismatch between the film and substrate is very large. This implies that for certain systems, it is possible that strain can be relaxed right at the interface during growth. Figure 1(b) illustrates the basic idea of strain-free vdWE. To date, there are many examples of successful vdWE of two-dimensional (2D) layered materials on 2D substrates.[9–15] More recently, it has been demonstrated that non-layered materials (or 3D materials) can also be epitaxially grown on weakly interacting vdW substrates.[16–31]

If an overlayer is completely relaxed without strains, it is called an incommensurate film.[3,5,8,29] In this paper, we propose a class of domain boundaries that is intrinsic to incommensurate films. They are natural consequences of random nucleation and incommensurability between the overlayer and substrate lattices. They exist in both a 2D layer and a 3D film. We demonstrate that the formation of those domain boundaries can be simulated with the Voronoi tessellation.[32] Various Voronoi patterns exist in nature such as biological cells, and Voronoi tessellation has been applied in many science and technology fields.[33] We compared our Voronoi tessellation simulated domain boundary with experimentally observed domain boundary in WS$_2$ monolayer epitaxially and unidirectionally grown on sapphire.[34]
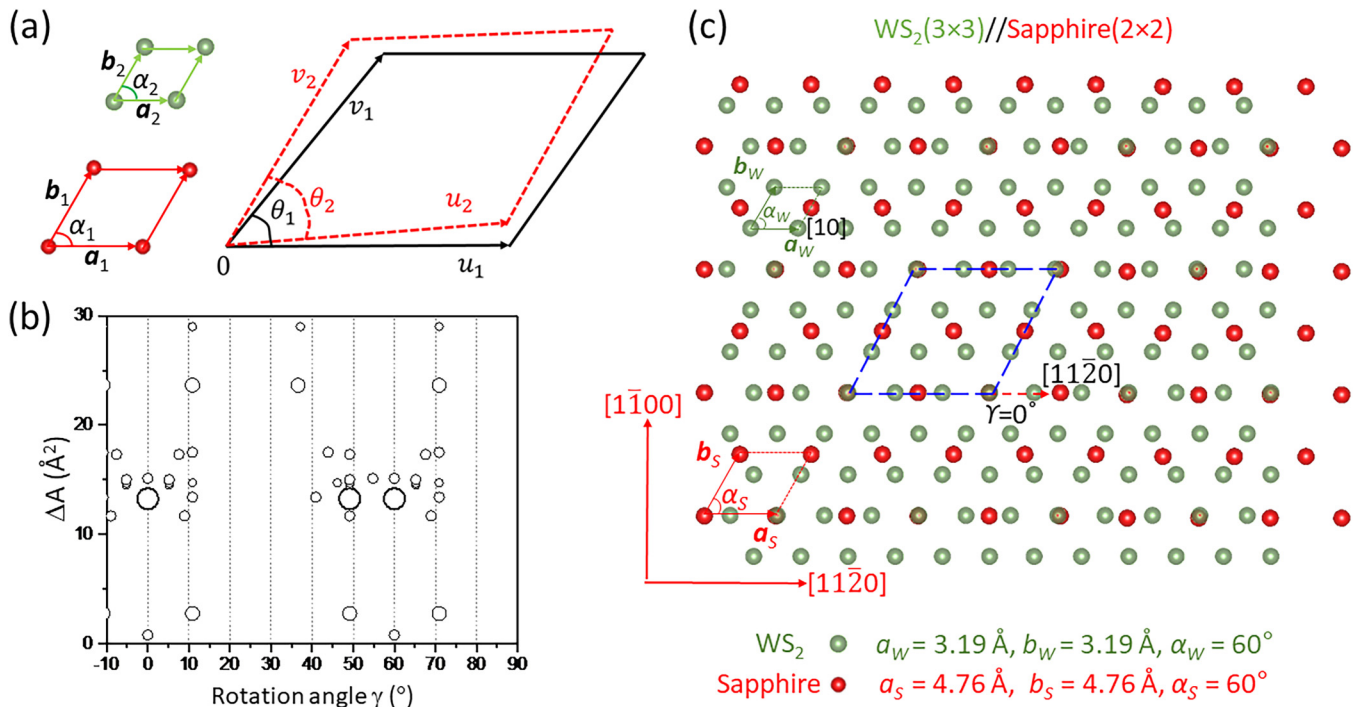
## II. GEOMETRICAL SUPERLATTICE AREA MISMATCH MODEL

Due to the lattice mismatch, especially the large mismatch systems, a superlattice structure (with respect to the substrate) often occurs in the overlayer. The occurrence of a particular superlattice structure depends on many factors including the energetics of the film–substrate interface. Prediction of the superlattice structures based on coincidence lattice matching has been proposed.[35] However, for a completely relaxed incommensurate film, a

geometrical superlattice area mismatch (GSAM) model is more appropriate to predict the likelihood of certain close superlattice structures.[21,36,37] In this model, the input parameters for an overlayer are in-plane lattice constants $a_2$, $b_2$, and the angle $\alpha_2$ between unit vectors $\boldsymbol{a}_2$ and $\boldsymbol{b}_2$. Similarly, the input parameters for a substrate are $a_1$, $b_1$, and the angle $\alpha_1$ between unit vectors $\boldsymbol{a}_1$ and $\boldsymbol{b}_1$. See the left panel in Fig. 2(a). The calculated superlattice structures are strain free and may not have an exact coincidence lattice matching but only a close coincidence lattice matching with the substrate. Therefore, the incommensurability of the overlayer remains intact. When two lattices form a heteroepitaxy, it is desirable to have a small superlattice area $A$ where the close coincidence superlattice matching density would be high. It is also desirable to have a small difference in areas, $\Delta A$, between the overlayer and substrate superlattices to minimize the system's energy. To incorporate these two considerations, a parameter called superlattice area mismatch, $\Delta A$, is defined as follows:[21,36,37]

$$\Delta A = A \left[ \frac{\Delta u}{u} + \frac{\Delta v}{v} + \frac{\Delta \theta}{\tan \theta} \right]. \quad (1)$$

Here, we define the sides of substrate superlattice as $u_1$ and $v_1$ with an angle $\theta_1$ between them and the sides of overlayer superlattice as $u_2$ and $v_2$ with an angle $\theta_2$ between them. This is illustrated graphically in Fig. 2(a). The superlattice mismatch is defined as $\Delta u \equiv u_2 - u_1$, $\Delta v \equiv v_2 - v_1$, and $\Delta \theta = \theta_2 - \theta_1$. $A_1$ and $A_2$ are the substrate and overlayer superlattice areas, respectively. For small superlattice mismatches, we have $u_2 \approx u_1 \equiv u$, $v_2 \approx v_1 \equiv v$, $\theta_2 \approx \theta_1 = \theta$, and $A_2 \approx A_1 = A$. In Eq. (1), $\Delta A$ can be regarded as a multiplication of two terms. The first term is $A$, which is inversely proportional to the close coincidence superlattice matching density. The second term is the square bracket that includes quantities proportional to the mismatch. Both terms need to be small to form a favorable interface. Therefore, a small $\Delta A$ value represents a favorable superlattice to be formed.

**FIG. 2.** (a) Overlayer unit mesh (green) with unit vectors $a_2$, $b_2$, and angle $\alpha_2$; substrate unit mesh (red) with unit vectors $a_1$, $b_1$, and angle $\alpha_1$; and superlattice with unit lengths $u_2$ and $v_2$, an angle $\theta_2$ between them and substrate superlattice with unit lengths $u_1$ and $v_1$, and an angle $\theta_1$ between them. (b) All calculated possible superlattice area differences $\Delta A$ (open circles) are plotted as a function of the relative rotation angle $\gamma$ between monolayer WS$_2$ and sapphire (0001). The maximum limits of $A$, $\frac{\Delta u}{u}$, $\frac{\Delta v}{v}$, and $\frac{\Delta \theta}{\theta}$ are set at 100 Å$^2$, 10%, 10%, and 10%, respectively. (c) The WS$_2$ and sapphire superlattice unit areas denoted as a blue dashed parallelogram for 0° rotation angle between 2D WS$_2$ [10] and sapphire [11$\bar{2}$0] directions.

We then use this criterion to determine the preferred superlattice structure of monolayer WS$_2$ on sapphire(0001) to illustrate the GSAM model calculation. Figure 2(b) shows the calculated result of all possible $\Delta A$ values using in-plane unit lattice constants of the sapphire substrate $a_s = b_s = 4.76$ Å, the angle $\alpha_s = 60°$ between the substrate units $a_s$ and $b_s$, in-plane unit lattice constants of the WS$_2$ overlayer $a_W = b_W = 3.19$ Å, and the angle $\alpha_w = 60°$ between the overlayer units $a_W$ and $b_W$, along the interface shown in Fig. 2(c). The maximum limits of $A$, $\frac{\Delta u}{u}$, $\frac{\Delta v}{v}$, and $\frac{\Delta \theta}{\theta}$ are 100 Å$^2$, 10%, 10%, and 10%, respectively. The radius of the circles in Fig. 2(b) is inversely proportional to $A$. The rotation angle $\gamma$ is defined as the angle between 2D WS$_2$ [10] and sapphire [11$\bar{2}$0] directions as shown in Fig. 2(c). In Fig. 2(b), we can identify that the smallest $\Delta A$ (0.82 Å$^2$) occurs at the rotation angle of $\gamma = 0°$ (equivalent to 60° due to the hexagonal lattice symmetry). Recently, this monolayer WS$_2$ on sapphire superlattice structure with a parallel epitaxy of $\gamma = 0°$ has been observed experimentally.[34] Parallel epitaxies were also observed in other transition metal dichalcogenide (TMDC) monolayers epitaxially grown on sapphire substrates.[38–42]
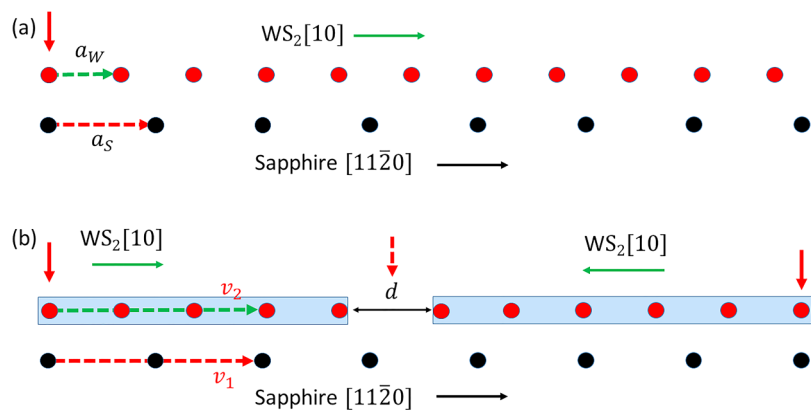
When superlattice domains nucleate at different nucleation sites in a lattice mismatched system, they inevitably form domain boundaries when domains grow and meet. For illustration purpose, consider a one-dimensional problem using monolayer WS$_2$ on sapphire as an example in Fig. 3. In Fig. 3(a), a single incommensurate WS$_2$ domain with a unit length $a_W$ is nucleated at the sapphire substrate with a unit length $a_s$ at the site indicated by the vertical red arrow and grows over the substrate. From the GSAM, Fig. 3(b) shows that the calculated superlattice unit lengths are $v_2 = 9.57$ Å (horizontal green dashed line) and and $v_1 = 9.52$ Å (horizontal red dashed line) for WS$_2$ [10] and sapphire [11$\bar{2}$0], respectively. In Fig. 3(b), in addition to the first nucleation site indicated by a vertical red arrow, a second nucleation site indicated by a vertical red arrow also occurs and forms a second domain. These two incommensurate domains grow laterally and meet at a boundary with a boundary width $d$, where $a_W < d < 2a_W$. The vertical red dashed arrow indicates the location of the boundary. If a compressive strain is allowed at the domain boundary, then $xa_W < d < 2a_W$ with $x$ smaller than 1. Note that within the domains themselves, they are still incommensurate and have no strain.

## III. DOMAIN BOUNDARIES FORMATION IN 2D USING VORONOI TESSELLATION

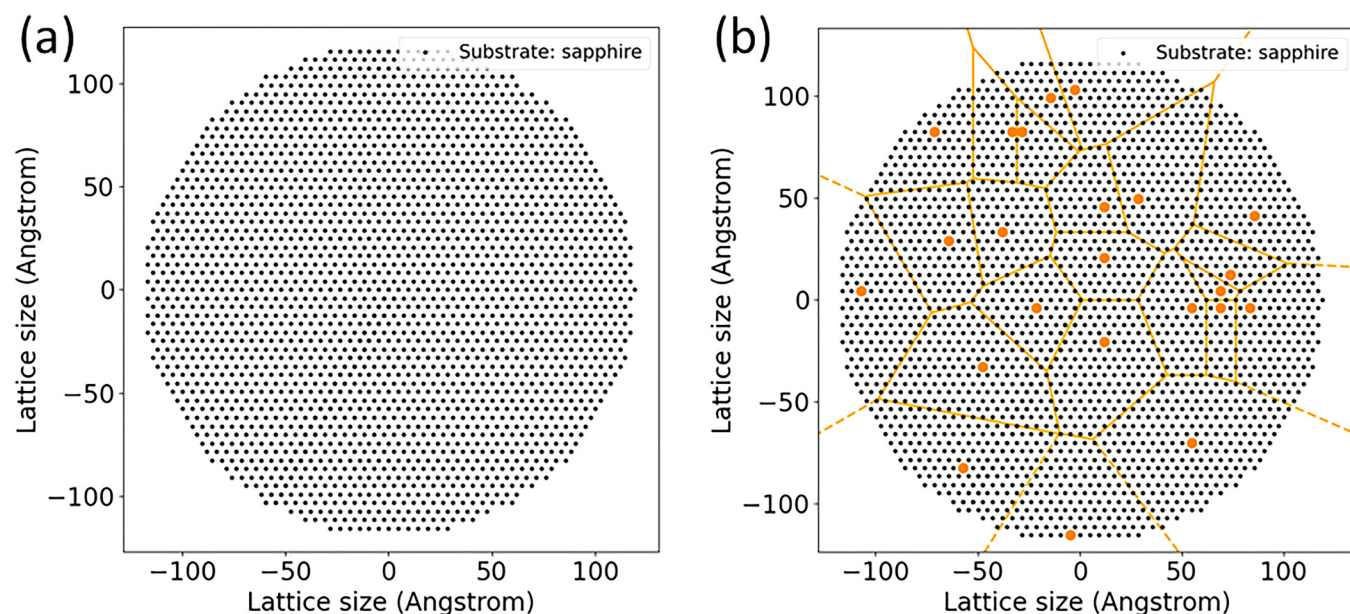### A. Nucleation centers and Voronoi tessellation on sapphire

In order to study the growth of domain regions and domain boundaries in the 2D case, we have utilized Python programming

**FIG. 3.** (a) A single WS$_2$ [10] incommensurate domain is nucleated at the site indicated by the vertical red arrow on the sapphire surface along the [11$\bar{2}$0] direction. $a_W$ and $a_s$ are unit lengths of the overlayer and the substrate, respectively. (b) In addition to the first nucleation site, a second nucleation site indicated by the vertical red arrow occurs and forms a second incommensurate domain. The two domains (blue shaded boxes) grow in the opposite directions indicated by the two green arrows and meet at a boundary with a boundary width $d$, where $a_W < d < 2a_W$, which is not equal to or smaller than $a_W$, the WS$_2$ lattice unit length in the [10] direction. $v_2$ and $v_1$ are unit lengths of overlayer superlattice and substrate superlattice, respectively.

language to simulate the domain boundaries formation numerically, using WS$_2$/sapphire as an example. We first create Voronoi domains on the sapphire substrate using Voronoi tessellation.[32,33] In the Python program, a substrate with a hexagonal pattern of sapphire is first created within the area of a circle. The size of the substrate lattice is determined by the number of lattice points within the circle's area of the sapphire substrate. Figure 4(a) illustrates a sapphire substrate lattice size in units of Å. The coordinates of all lattice points on the substrates are stored in a list for later use. The program randomly picks a small portion of the coordinates of the lattice points that are stored in the list, which will act as the nucleation centers for later overlayer domain growth. This portion is what we call the density of nucleation sites. The domain boundaries are then constructed via Voronoi tessellation. The Voronoi tessellation partitions the plane of a substrate into different regions (domains), one nucleation site per domain. A domain boundary is the bisector between adjacent nucleation sites. Each nucleation site will have an associated domain consisting of all lattice points closer to that nucleation site than to any other nucleation sites. Figure 4(b) illustrates the domain regions (orange polygons) with their respective nucleation sites (orange dots) with a density of 0.8% on the sapphire substrate lattice points. The domains have an irregular polygon shape. Depending on the location of the nucleation sites, many different domain boundaries can be formed. Note that at this point, the domain boundaries are imaginary boundaries on the sapphire surface and no overlayer has been added yet.



**FIG. 4.** (a) Lattice of sapphire (0001) substrate for Voronoi simulation. (b) The Voronoi domain regions (orange polygons) with their respective nucleation sites (orange dots) on the sapphire lattice. For each nucleation site, the domain region consists of all lattice points in the plane closer to that site than to any other nucleation sites.

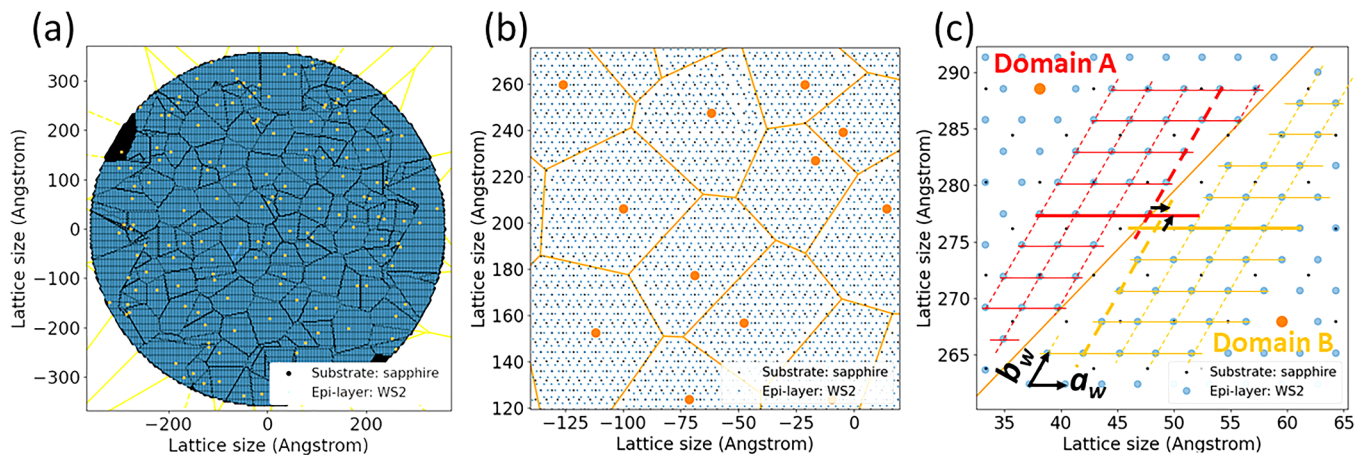## B. Domains and domain boundaries in WS$_2$ monolayer on sapphire

With the nucleation centers and domain boundaries identified, the next step is to fill each domain with the overlayer lattice. This model considers a multistep growth process starting with a set of randomly chosen nucleation sites and followed by the lateral growth. The nucleation was diffusion-limited while the lateral growth was nucleation-limited.[34,40] Overlayer lattice points from the nuclei in all domains are assumed to start filling or growing simultaneously. The growth front of each domain is assumed to be isotropic (expands circularly). If there is a spatial diffusion anisotropy, anisotropic Voronoi tessellation can be applied.[43] It will affect the shape of the cells but does not affect the average domain size (the average domain size is inversely proportional to the nucleation density) and the types of domain boundaries. The WS$_2$ lattice is of hexagonal shape and the overlayer with its own lattice constants ($a_w = b_w = 3.19$ Å) is grown parallel to the hexagonal sapphire substrate lattice ($a_s = b_s = 4.76$ Å). Intuitively, WS$_2$ lattices are filled as densely as possible into each domain. If there is no strain at the boundaries, two WS$_2$ lattice points on each side of the domain boundary cannot be less than one lattice constant (3.19 Å). Therefore, an elimination of lattice points that are too close to each other is needed. The elimination proceeds as follows. Epitaxial WS$_2$ lattice points are filled into each domain one by one. For each lattice point to be filled into the current domain, its closest distance to any lattice point within the previous domain will be calculated. If this distance is smaller than one lattice constant of WS$_2$, that pending lattice point will not be filled into the current domain. The process continues until all the regions are filled with WS$_2$ and the simulation of WS$_2$ epitaxial layer growth on sapphire is completed. Figure 5(a) shows a simulated epitaxial WS$_2$ monolayer grown on sapphire with a nucleation density of 0.8%. The sapphire

substrate has 20 551 lattice points in total, which covers a circular area with a radius of ~350 Å. The sapphire lattice points are in black, the WS$_2$ lattice points are in blue, and the nucleation centers are in orange. The WS$_2$ domain boundaries are outlined in black color. Figure 5(b) shows a zoom-in area (~150 × 150 Å$^2$) illustrating multiple WS$_2$ domains with highlighted Voronoi domain boundaries and nucleation centers both in orange. The structure of a typical WS$_2$ domain boundary is shown in Fig. 5(c). The two domains in Fig. 5(c) are labeled as "Domain A" and "Domain B" with both nucleation centers highlighted in orange dots. Solid and dashed lines are drawn on the WS$_2$ lattice near the domain boundary along unit mesh $a_w$ and $b_w$ directions with an angle of $\alpha_w = 60°$. To distinguish these two domains with the same orientation, the lightweight solid and dashed lines connecting WS$_2$ lattice sites are drawn in red for domain A and yellow color for domain B.
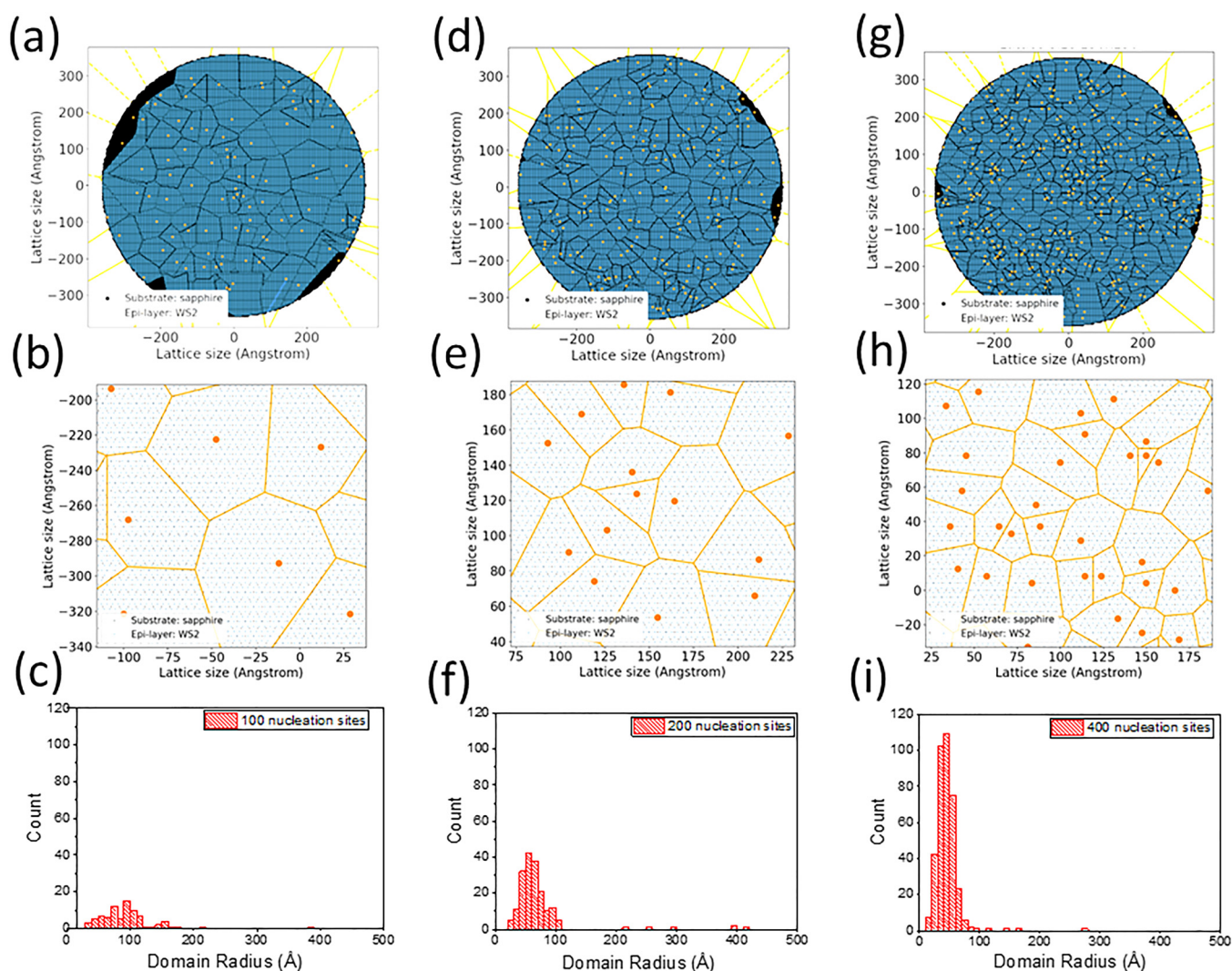
As one can see in Fig. 5(c), WS$_2$ lattice in domain A are not well aligned with the lattice in domain B, and they are translated in both $a_w$ and $b_w$ directions as indicated by the two black arrows near the boundary. That is a translational shift from the heavy horizontal solid red line to the heavy horizontal solid orange line along the $b_w$ direction. Similarly, a translational shift occurs from the heavy dashed red line to the heavy dashed orange line along the $a_w$ direction. The translation in the $a_w$ direction is about 52% of the WS$_2$ lattice constant, and the translation is about 43% in the $b_w$ direction. Because the distance between two lattices on the opposite sides of the domain boundary is smaller than one lattice constant of WS$_2$, one of the lattice sites is eliminated along the domain boundary, shown as voids in the diagram.

## C. Nucleation density dependent domain sizes

To investigate the effect of nucleation density on the domain size, we have carried out three more simulations with 0.5%, 1.0%,



**FIG. 5.** (a) A schematic shows simulated Voronoi domains of epitaxial WS$_2$ monolayer on sapphire with nucleation site density of 0.8%. The orange dots represent nucleation sites. WS$_2$ lattice sites are represented by blue dots and sapphire lattice sites are represented by black dots. The entire sapphire lattice area is 150 × 150 lattice points (~710 × 710 Å$^2$). (b) A selected zoom-in area showing the WS$_2$ nucleation sites (orange dots) and domain boundaries (orange lines). The lattice area is ~150 × 150 Å$^2$. (c) A schematic showing the detailed structure of a particular domain boundary. The orange and red solid and dashed lines parallel to unit vectors $a_w$ and $b_w$ directions connect lattice points in domain A and domain B, respectively. The misalignment of the yellow and red lines in $a_w$ and $b_w$ directions indicates translational mismatch in both directions across the domain boundary represented by an orange line.
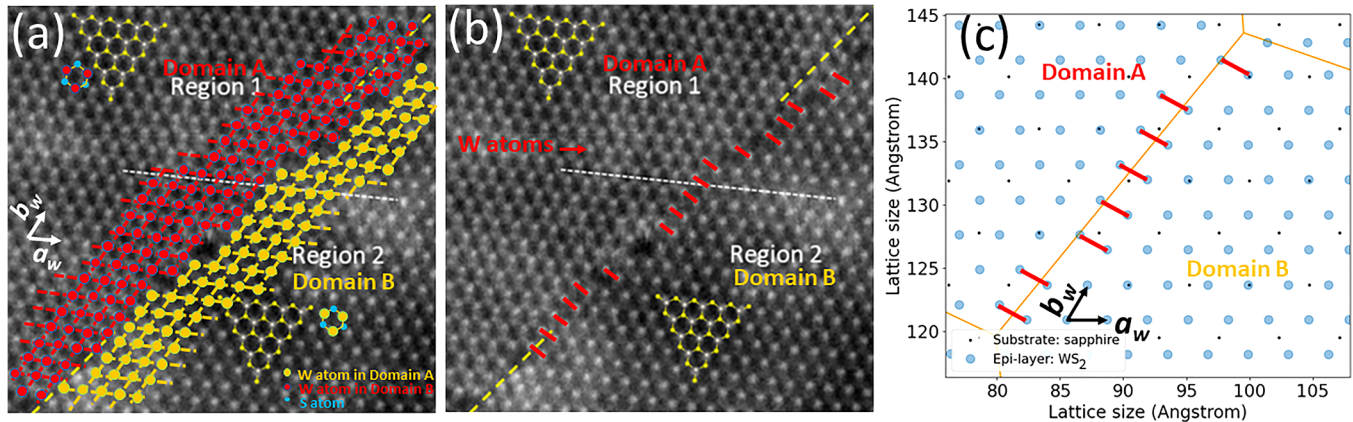
**FIG. 6.** (a), (d), and (g) Voronoi domains of the WS$_2$ lattice on sapphire lattice with nucleation site densities of 0.5% (100 sites), 1.0% (200 sites), and 2.0% (400 sites). The entire sapphire lattice area is 150 × 150 lattice points (~710 × 710 Å$^2$). (b), (e), and (h) The corresponding selected zoom-in areas (~150 × 150 Å$^2$) of (a), (d), and (g) as a function of the nucleation site density. (c), (f), and (i) The histograms of the distribution of average domain size (domain radius) as a function of the nucleation site density extracted from (a), (d), and (g).

and 2.0% nucleation densities. Figures 6(a), 6(d), and 6(g) are three Voronoi domain plots with the nucleation densities of ~0.5% (100 nucleation sites), ~1.0% (200 nucleation sites), and ~2.0% (400 nucleation sites) with the same substrate lattice dimensions (radius ~350 Å) as used before. Note that all the domain boundaries are translational boundaries with 0° relative in-plane orientation rotation. The dark regions at the edge of the circles are the regions where the boundaries are not intersected by an adjacent boundary. Figures 6(b), 6(e), and 6(h) are corresponding zoom-in areas for Figs. 6(a), 6(d), and 6(g), respectively. Qualitatively, one can see that with the increase of nucleation site density, the size of the WS$_2$ domains decreases accordingly. Here, we define the domain radius

as the square root of the area of this domain. Figures 6(c), 6(f), and 6(i) are the histograms of domain radius corresponding to Figs. 6(a), 6(d), and 6(g). All three histogram plots show a tendency of negative binomial distribution, with the maximum domain size that occurs around a domain radius of ~90, ~55, and ~45 Å, respectively. The average domain radii are 95 ± 46, 70 ± 53, and 45 ± 19 Å for Figs. 6(c), 6(f), and 6(i), respectively.

## IV. EXPERIMENTAL REALIZATION IN THE WS$_2$ MONOLAYER ON SAPPHIRE

A recent work of epitaxial WS$_2$ monolayer grown by metalorganic chemical vapor deposition on sapphire shows a wafer scale

**FIG. 7.** (a) A reported high-resolution transmission electron microscopy (HRTEM) image of the monolayer $WS_2$ epitaxially grown on a sapphire(0001) wafer.[34] Reprinted with permission from Chubarov *et al.*, ACS Nano **15**, 2532 (2021). Copyright 2021 American Chemical Society. The bright spots and the dim spots correspond to W atoms and S atoms, respectively. Along the domain boundary, W atoms in domain A and domain B are masked with red and yellow dots across the domain boundary, respectively. Domain A and domain B are incommensurate and have the same in-plane crystalline orientation. The yellow and red dashed lines are parallel to lattice unit vector $a_w$ and $b_w$ directions. The misalignment of the yellow and red dashed lines in $a_w$ and $b_w$ directions indicate translational mismatches in both directions across the boundary. The white dotted line indicates a translational shift of domain in the $b_w$ direction. (b) In the same HRTEM image, pairs of W atoms with the distance shorter than one lattice constant (3.19 Å) across the boundary are linked with red lines indicating a compressive strain across the boundary. The measured distance is $2.35 \pm 0.13$ Å. This average distance is $26.3 \pm 0.41\%$ shorter than one lattice constant of 3.19 Å. (c) A simulated Voronoi diagram showing the detailed structure of a particular domain boundary similar to the experiment data shown in (b). Pairs of $WS_2$ lattice points with the distance shorter than one lattice constant across the boundary are linked with red lines indicating a similar compressive strain across the boundary. The average distance is $24.5 \pm 1.3\%$ shorter than one lattice constant 3.19 Å.

unidirectional $WS_2$ monolayer on sapphire. Figure 7(a) shows a high-resolution transmission electron microscopy (HRTEM) image of the $WS_2$ monolayer transferred to a TEM grid.[34] In the original TEM image, the authors highlighted the grain boundary by two yellow dashed lines, the same orientation domains in region 1 and region 2 with the superposed $WS_2$ structure, and a white dashed line for translational offset between regions 1 and 2. The bright spots correspond to W atoms (which we treated as a lattice point), and the dim spots correspond to S atoms. We added red and yellow solid circles superposed on W sites in domain A (region 1) and domain B (region 2), respectively. Now the domain boundary with voids and misalignment of domain A and domain B are more obvious. Domain A and domain B are incommensurate with respect to the substrate and have the same in-plane crystalline orientation. The yellow and red dashed line directions align with lattice unit vector $a_w$ and $b_w$ directions. The misalignment of the yellow and red dashed lines in $a_w$ and $b_w$ directions indicate translational mismatches in both directions near the boundary. Upon a closer examination of the image in Fig. 7(b), we labeled pairs of W atoms with red lines that have distances shorter than one lattice constant across the boundary. These indicate a compressive strain situation across the boundary. The measured average distance of red lines is $2.35 \pm 0.13$ Å. This average distance is $26.3 \pm 4.1\%$ shorter than one lattice constant of 3.19 Å.

To account for a possible strain at the boundaries, a simulated Voronoi diagram that allows the nearest lattice distance smaller than one lattice constant $a_w = b_w = 3.19$ Å but larger than half of the lattice constant at the boundaries was simulated. Figure 7(c) shows the detailed structure of a particular domain boundary similar to the experimental TEM image shown in Fig. 7(b). Pairs of

$WS_2$ lattice points with the distances shorter than one lattice constant (3.19 Å) across the boundary are linked with red lines indicating the same compressive strain situation across the boundary. The average distance of red lines is $24.5 \pm 1.3\%$ shorter than one lattice constant of 3.19 Å.

Note that incommensurate domain boundaries differ from the conventional dislocations that result from the relaxation of strain due to film–substrate lattice mismatch in a film. No strain is considered in an individual incommensurate domain in the film. However, the domains in the domain matching epitaxy models,[44–46] for example, that were used to explain large lattice mismatch systems with strong film–substrate chemical interactions do possess strains. These strains induced by film–substrate interactions would generate dislocations in the film. Due to the matching of integral multiples of lattice constants between the film and substrate, the strain could be small, but nevertheless it still exists. In the current model, there is no strain in the individual incommensurate domain due to film–substrate interaction and no dislocation is generated in the domain due to strain. The strains at the incommensurate domain boundaries discussed here are a result of the compressive squeezing between the adjacent overlayer incommensurate domains when they meet to form a boundary with the boundary distance $d$ smaller than one overlayer lattice constant. This strain is not induced by the film–substrate interactions.

## V. CONCLUSION

We have argued that for an incommensurate epitaxial film, intrinsic domain boundaries can exist due to the random nucleation of overlayer domains on a lattice mismatched substrate. We

use the Voronoi tessellation method to simulate the creation of domain boundaries in an epitaxial layer. Epitaxial growth of monolayer $WS_2$ on the sapphire surface has been used as a model system to illustrate the idea. The simulated domain boundaries compare well with HRTEM observations. Rich domain boundaries with different structures are created, which is a function of the density of nucleation sites. Domain boundaries should exist in 2D on 3D or 3D on 2D incommensurate films with random nucleation sites. By reducing the nucleation density, one can obtain larger domain sizes. Also, even if the nucleation is not random, when domains meet, translational boundaries should still be created. This is a result of the incommensurability of the overlayer with respect to the substrate, especially when there is a large lattice constant mismatch between the overlayer and the substrate.

## ACKNOWLEDGMENTS

## DATA AVAILABILITY

The data that support the findings of this study are available from the corresponding author upon reasonable request.

## REFERENCES

[1]J. E. Ayers, *Heteroepitaxy of Semiconductors: Theory, Growth, and Characterization* (CRC Press, Boca Raton, FL, 2016).

[2]A. Koma, "Van der Waals epitaxy—A new epitaxial growth method for a highly lattice-mismatched system," Thin Solid Films **216**, 72 (1992).

[3]M. I. B. Utama, Q. Zhang, J. Zhang, Y. Yuan, F. J. Belarre, J. Arbiol, and Q. Xiong, "Recent developments and future directions in the growth of nanostructures by van der Waals epitaxy," Nanoscale **5**, 3570 (2013).

[4]J. J. Lander and J. Morrison, "A LEED investigation of physisorption," Surf. Sci. **6**, 1 (1967).

[5]J. D. Dash, *Films on Solid Surfaces* (Academic Press, New York, 1975).

[6]A. D. Novaco and J. P. McTague, "Orientational epitaxy—The orientational ordering of incommensurate structures," Phys. Rev. Lett. **38**, 1286 (1977).

[7]C. G. Shaw, S. C. Fain, and M. D. Chinn, "Observation of orientational ordering of incommensurate argon monolayers on graphite," Phys. Rev. Lett. **41**, 955 (1978).

[8]A. Koma, "Van der Waals epitaxy for highly lattice-mismatched systems," J. Cryst. Growth **201–202**, 236 (1999).

[9]A. K. Geim and I. V. Grigorieva, "Van der Waals heterostructures," Nature **499**, 419 (2013).

[10]T. Björkman, A. Gulans, A. V. Krasheninnikov, and R. M. Nieminen, "Van der Waals bonding in layered compounds from advanced density-functional first-principles calculations," Phys. Rev. Lett. **108**, 235502 (2012).

[11]K. K. Leung, W. Wang, H. Shu, Y. Y. Hui, S. Wang, P. W. K. Fong, F. Ding, S. P. Lau, C.-h. Lam, and C. Surya, "Theoretical and experimental investigations on the growth of SnS van der Waals epitaxies on graphene buffer layer," Cryst. Growth Des. **13**, 4755 (2013).

[12]J. E. Boschker, L. A. Galves, T. Flissikowski, J. M. J. Lopes, H. Riechert, and R. Calarco, "Coincident-site lattice matching during van der Waals epitaxy," Sci. Rep. **5**, 18079 (2016).

[13]B. Li, X. Guo, W. Ho, and M. Xie, "Strain in epitaxial $Bi_2Se_3$ grown on GaN and graphene substrates: A reflection high-energy electron diffraction study," Appl. Phys. Lett. **107**, 081604 (2015).

[14]A. Azizi, S. Eichfeld, G. Geschwind, K. Zhang, B. Jiang, D. Mukherjee, L. Hossain, A. F. Piasecki, B. Kabius, J. A. Robinson, and N. Alem, "Freestanding van der Waals heterostructures of graphene and transition metal dichalcogenides," ACS Nano **9**, 4882 (2015).

[15]H. Ago, Y. Ohta, H. Hibino, D. Yoshimura, R. Takizawa, Y. Uchida, M. Tsuji, T. Okajima, H. Mitani, and S. Mizuno, "Growth dynamics of single-layer graphene on epitaxial Cu surfaces," Chem. Mater. **27**, 5377 (2015).

[16]Y. Alaskar, S. Arafin, D. Wickramaratne, M. A. Zurbuchen, L. He, J. McKay, Q. Lin, M. S. Goorsky, R. K. Lake, and K. L. Wang, "Towards van der Waals epitaxial growth of GaAs on Si using a graphene buffer layer," Adv. Funct. Mater. **24**, 6629 (2014).

[17]J. Kim, C. Bayram, H. Park, C.-W. Cheng, C. Dimitrakopoulos, J. A. Ott, K. B. Reuter, S. W. Bedell, and D. K. Sadana, "Principle of direct van der Waals epitaxy of single-crystalline films on epitaxial graphene," Nat. Commun. **5**, 4836 (2014).

[18]Y. Jung, G. Yang, S. Chun, D. Kim, and J. Kim, "Growth of CdTe thin films on graphene by close-spaced sublimation method," Appl. Phys. Lett. **103**, 231910 (2013).

[19]G. Yang, D. Kim, and J. Kim, "Self-aligned growth of CdTe photodetectors using a graphene seed layer," Optics Express **23**, A1081 (2015).

[20]D. Mohanty, Z. Lu, X. Sun, Y. Xiang, Y. Wang, D. Ghoshal, J. Shi, L. Gao, S. Shi, M. Washington, G.-C. Wang, T.-M. Lu, and I. Bhat, "Metalorganic vapor phase epitaxy of large size CdTe grains on mica through chemical and van der Waals interactions," Phys. Rev. Mater. **2**, 113402 (2018).

[21]X. Sun, Z. Lu, W. Xie, Y. Wang, J. Shi, S. Zhang, M. A. Washington, and T.-M. Lu, "Van der Waals epitaxy of CdS thin films on single-crystalline graphene," Appl. Phys. Lett. **110**, 153104 (2017).

[22]X. Sun, Z. Chen, Y. Wang, Z. Lu, J. Shi, M. Washington, and T.-M. Lu, "Van der Waals epitaxial ZnTe thin film on single-crystalline graphene," J. Appl. Phys. **123**, 025303 (2018).

[23]X. Sun, Z. Lu, Z. Chen, Y. Wang, J. Shi, M. Washington, and T.-M. Lu, "Single-crystal graphene-directed van der Waals epitaxial resistive switching," ACS Appl. Mater. Interfaces **10**, 6730 (2018).

[24]X. Sun, Z. Lu, Y. Xiang, Y. Wang, J. Shi, G.-C. Wang, M. A. Washington, and T.-M. Lu, "Van der Waals epitaxy of antimony islands, sheets, and thin films on single-crystalline graphene," ACS Nano **12**, 6100 (2018).

[25]Z. Lu, X. Sun, M. A. Washington, and T.-M. Lu, "Quasi van der Waals epitaxy of copper thin film on single-crystal graphene monolayer buffer," J. Phys. D: Appl. Phys. **51**, 095301 (2018).

[26]S. Pendse, J. Jiang, Y. Guo, L. Zhang, Z. Chen, Z. Lu, Y. Wang, S. Li, J. Feng, T.-M. Lu, Y.-Y. Sun, and J. Shi, "Unit-cell-thick oxide synthesis by film-based scavenging," J. Phys. Chem. C **124**, 8394 (2020).

[27]S. Pendse, J. Jiang, L. Zhang, Y. Guo, Z. Chen, Y. Hu, Z. Lu, S. Li, J. Feng, T.-M. Lu, and J. Shi, "Tuning phase transition kinetics via van der Waals epitaxy of single crystalline $VO_2$ on hexagonal-BN," J. Cryst. Growth **543**, 125699 (2020).

[28]Y. Wang, L. Gao, Y. Yang, Y. Xiang, Z. Chen, Y. Dong, H. Zhou, Z. Cai, G.-C. Wang, and J. Shi, "Nontrivial strength of van der Waals epitaxial interaction in soft perovskites," Phys. Rev. Mater. **2**, 076002 (2018).

[29]Y. Wang, X. Sun, R. Shivanna, Y. Yang, Z. Chen, Y. Guo, G.-C. Wang, E. Wertz, F. Deschler, Z. Cai, H. Zhou, T.-M. Lu, and J. Shi, "Photon transport in one-dimensional incommensurately epitaxial $CsPbX_3$ arrays," Nano Lett. **16**(12), 7974–7981 (2016).

[30]X. Wen, Z. Lu, X. Sun, Y. Xiang, Z. Chen, J. Shi, I. Bhat, G.-C. Wang, M. Washington, and T.-M. Lu, "Epitaxial CdTe thin films on mica by vapor transport deposition for flexible solar cells," ACS Appl. Energy Mater. **3**, 4589 (2020).

[31]X. Wen, Z. Lu, L. Valdman, G.-C. Wang, M. Washington, and T.-M. Lu, "High-crystallinity epitaxial $Sb_2Se_3$ thin films on mica for flexible near-infrared photodetectors," ACS Appl. Mater. Interfaces **12**, 35222 (2020).

[32]R. Subrata and A. Y. Zomaya, "Some results on the computation of Voronoi diagrams on a mesh with multiple broadcasting," J. Parallel Distrib. Comput. **63**, 1300 (2003).

[33]F. Aurenhammer, R. Klein, and D.-T. Lee, *Voronoi Diagrams and Delaunay Triangulations* (World Scientific, 2013).

[34]M. Chubarov, T. H. Choudhury, D. R. Hickey, S. Bachu, T. Zhang, A. Sebastian, A. Bansal, H. Zhu, N. Trainor, S. Das, M. Terrones, N. Alem, and J. M. Redwing, "Wafer-scale epitaxial growth of unidirectional WS$_2$ monolayers on sapphire," ACS Nano **15**, 2532 (2021).

[35]D. S. Koda, F. Bechstedt, M. Marques, and L. K. Teles, "Coincidence lattices of 2D crystals: Heterostructure predictions and applications," J. Phys. Chem. C **120**, 10895 (2016).

[36]A. S. Yapsir, C. H. Choi, and T.-M. Lu, "Observation of a new Al(111)/Si(111) orientational epitaxy," J. Appl. Phys. **67**, 796 (1990).

[37]A. Zur and T. C. McGill, "Lattice match: An application to heteroepitaxy," J. Appl. Phys. **55**, 378 (1984).

[38]D. Dumcenco, D. Ovchinnikov, K. Marinov, P. Lazić, M. Gibertini, N. Marzari, O. L. Sanchez, Y.-C. Kung, D. Krasnozhon, M.-W. Chen, S. Bertolazzi, P. Gillet, A. Fontcuberta i Morral, A. Radenovic, and A. Kis, "Large-area epitaxial monolayer MoS$_2$," ACS Nano **9**, 4611 (2015).

[39]H. Yu, M. Liao, W. Zhao, G. Liu, X. J. Zhou, Z. Wei, X. Xu, K. Liu, Z. Hu, K. Deng, S. Zhou, J.-A. Shi, L. Gu, C. Shen, T. Zhang, L. Du, L. Xie, J. Zhu, W. Chen, R. Yang, D. Shi, and G. Zhang, "Wafer-Scale growth and transfer of highly-oriented monolayer MoS$_2$ continuous films," ACS Nano **11**, 12001 (2017).

[40]X. Zhang, T. H. Choudhury, M. Chubarov, Y. Xiang, B. Jariwala, F. Zhang, N. Alem, G.-C. Wang, J. A. Robinson, and J. M. Redwing, "Diffusion-controlled epitaxy of large area coalesced WSe$_2$ monolayers on sapphire," Nano Lett. **18**, 1049 (2018).

[41]Y.-C. Lin, B. Jariwala, B. M. Bersch, K. Xu, Y. Nie, B. Wang, S. M. Eichfeld, X. Zhang, T. H. Choudhury, Y. Pan, R. Addou, C. M. Smyth, J. Li, K. Zhang, M. A. Haque, S. Fölsch, R. M. Feenstra, R. M. Wallace, K. Cho, S. K. Fullerton-Shirey, J. M. Redwing, and J. A. Robinson, "Realizing large-scale, electronic-grade two-dimensional semiconductors," ACS Nano **12**, 965 (2018).

[42]Y. Xiang, X. Sun, L. Valdman, F. Zhang, T. H. Choudhury, M. Chubarov, J. A. Robinson, J. M. Redwing, M. Terrones, Y. Ma, L. Gao, M. A. Washington, T.-M. Lu, and G.-C. Wang, "Monolayer MoS$_2$ on sapphire: An azimuthal reflection high-energy electron diffraction perspective," 2D Mater. **8**, 025003 (2021).

[43]T. F. W. van Nuland, J. A. W. van Dommelen, and M. G. D. Geers, "An anisotropic Voronoi algorithm for generating polycrystalline microstructures with preferred growth directions," Comput. Mater. Sci. **186**, 109947 (2021).

[44]J. Narayan, "Recent progress in thin film epitaxy across the misfit scale (2011 Acta Gold Medal Paper)," Acta Mater. **61**, 2703 (2013).

[45]J. Narayan and B. C. Larson, "Domain epitaxy: A unified paradigm for thin film growth," J. Appl. Phys. **93**, 278 (2003).

[46]W. Xie, M. Lucking, L. Chen, I. Bhat, G.-C. Wang, T.-M. Lu, and S. Zhang, "Modular approach for metal–semiconductor heterostructures with very large interface lattice misfit: A first-principles perspective," Cryst. Growth Des. **16**, 2328 (2016).